Precambrian Research 378 (2022) 106734

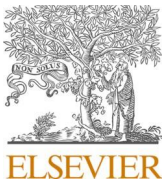

Contents lists available at ScienceDirect

Precambrian Research

journal homepage: www.elsevier.com/locate/precamres

Enigmatic provenance of carbonate clasts in Cryogenian glacial diamictite of the Nantuo Formation in South China

Morrison Nolan, Shuhai Xiao *, Benjamin Gill, Rachel Reid, Maxwel Schwid

Department of Geosciences, Virginia Tech, Blacksburg, VA 24061, USA

ARTICLE INFO

Keywords:
Carbon isotopes and oxygen isotopes
Sediment provenance
Carbonate clasts
Cryogenian glacial diamictite
Yangtze Craton
Nantuo Formation

ABSTRACT

Glacial diamictites of the Cryogenian Nantuo Formation of the Yangtze Craton of South China record major environmental transitions during the Marinoan glaciation. Although the provenance of the siliciclastic materials in the Nantuo Formation have been constrained via detrital zircon analysis, the source areas for the abundant carbonate clasts within the formation have yet to be determined. Given that the Mesoproterozoic Shennongjia Group is the only major extant pre-Cryogenian sedimentary carbonate succession in South China, it has been proposed as a source of the Nantuo dolostone clasts in the northern Yangtze Craton and may have been a major supplier of Cryogenian carbonate clasts across the entire Yangtze Craton, but this speculative provenance has not been tested or formally investigated. To test this hypothesis, $\delta^{13}C$ and $\delta^{18}O$ values of 18 clasts collected near Yichang, Hubei Province were analyzed along with petrographic examination to determine lithology, diagenetic alteration, and relationship to the Shennongjia Group carbonates. Our data show that the $\delta^{18}O$ and $\delta^{13}C$ values of these clasts are distinct from and thus unlikely sourced from the Shennongjia Group. Therefore, the Shennongjia Group cannot be the sole source of Nantuo carbonate clasts. Instead, we propose the Nantuo carbonate clasts in the study area were derived from either (1) pre-Marinoan carbonate successions in South China that were lost due to erosion or (2) another craton (e.g., the Indian Craton) adjacent to the Yangtze Craton during the Cryogenian. Given that paleogeographic and detrital zircon provenance analysis suggest separation between the Yangtze Craton and the Indian Craton in the Cryogenian Period, we favor the former origin, and that the Shennongjia Group is not the exclusive source of carbonate clasts from the Nantuo Formation.

1. Introduction

The terminal Cryogenian Nantuo Formation, a succession of glacial diamictite and siliciclastic rocks, archives important sedimentological, geochemical and paleontological data regarding environmental conditions and biological evolution during the Marinoan glaciation (Fig. 1A-B) (Chen et al., 2021; Hu et al., 2020; Lang et al., 2018). For example, sedimentary cycles in the Nantuo Formation indicate dynamic environmental changes including episodes of glacial advances and retreats (Chen et al., 2021; Hu et al., 2012a, 2020; Shen et al., 2021). During these advances and retreats, abundant sediment clasts were eroded and entrained into glacial diamictites. These clasts were mostly derived from igneous and metamorphic rocks, but carbonate clasts are common (Luo, 2015; Sha et al., 1963). Carbonate rocks of the Mesoproterozoic Shennongjia Group in the Shennongjia area are frequently suggested as the potential source of the carbonate clasts in the Nantuo Formation, at least in the northern Yangtze Craton near the Shennongjia area (Lu et al., 1985; Lu and Qu, 1985; Zhao et al., 2018). Given that the Shennongjia Group is the only major extant pre-Cryogenian carbonate-bearing succession in South China, it is plausible to hypothesize that the Shennongjia Group may have supplied the carbonate clasts in the Nantuo Formation across the entire Yangtze Craton. However, this hypothesized provenance has not been formally investigated. Elucidating the provenance of these clasts can be useful in determining the extent and intensity of the local glacial advances and retreats, for example the evaluation of glacial transport distance. In this study, we present new petrographic and $\delta^{13}C$ and $\delta^{18}O$ data to determine whether the Nantuo carbonate clasts are consistent with an origin from the Shennongjia Group. The rationale of this study is simple: if the carbonate clasts were derived from the Shennongjia Group, their petrographic features and isotopic signatures should be similar to those of the source rock, unless they experienced post-reworking diagenetic alteration, which can be assessed by examining the geochemical transects across the clasts because clast exterior is expected to be more susceptible to interaction

* Corresponding author.
E-mail address: xiao@vt.edu (S. Xiao).

https://doi.org/10.1016/j.precamres.2022.106734
Received 4 January 2022; Received in revised form 12 May 2022; Accepted 13 May 2022

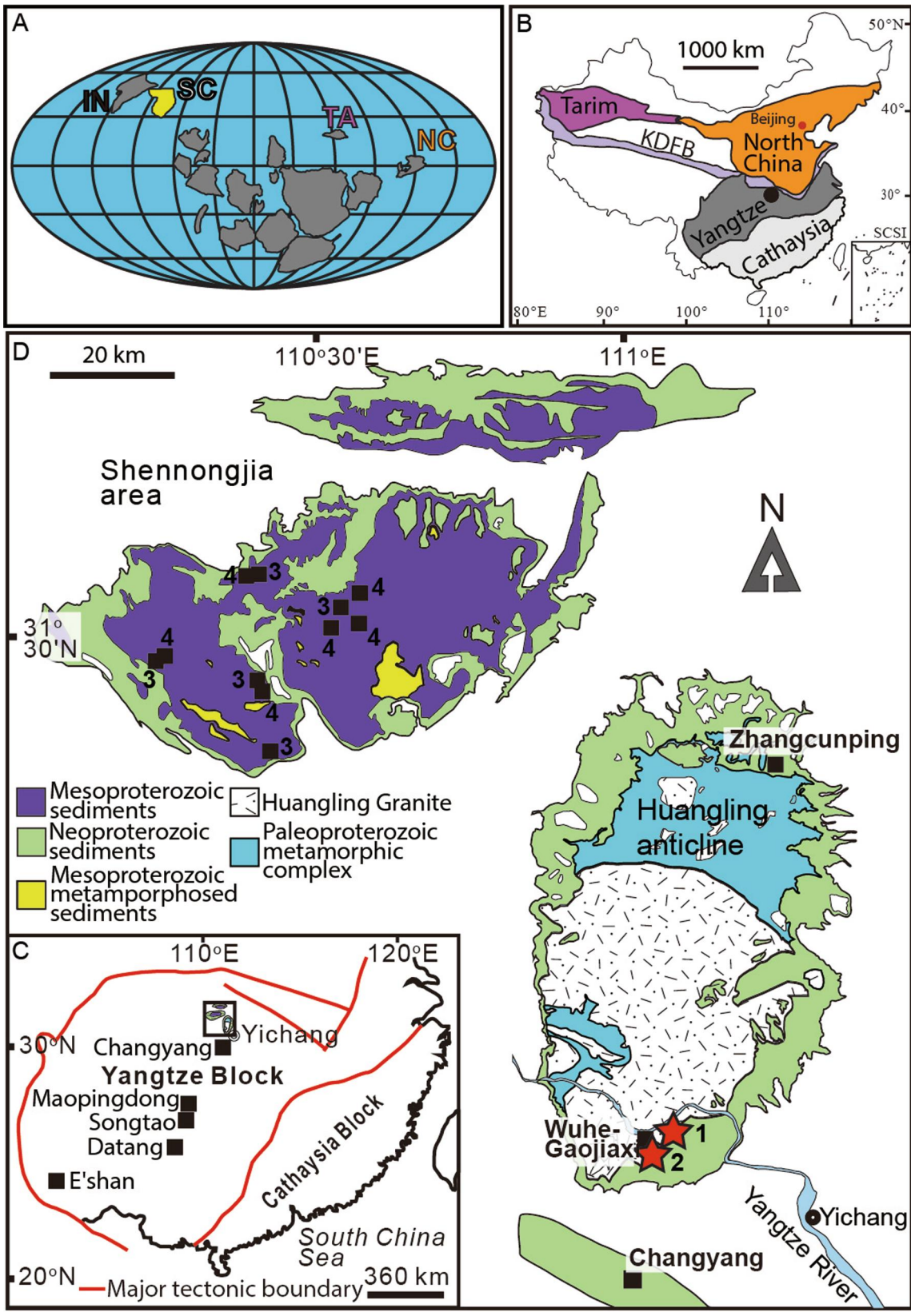

Fig. 1. Geographic and geologic context. (A) Terminal Cryogenian (~635 Ma) paleogeographic reconstruction: IN–India, TA–Tarim, NC–North China, and SC–South China (Yangtze and Cathaysia blocks). Adapted from Bao et al. (2018). (B) Major cratons in China, with study area marked by black dot; adapted from Liu et al. (2014). KDFB – Kunlun-Dabie Fold Belt, SCSI – South China Sea Islands. (C) Map of Yangtze and Cathaysia blocks, with rectangle marking Huangling anticline and Shennongjia area. (D) Geological map of the Huangling anticline and Shennongjia area. Black squares in (C–D) denote localities mentioned in text and in Fig. 7. Black squares labeled "3″ in (D), Shennongjia Group sections in Shennongjia area (Zou et al., 2019); black squares labeled "4" in (D), Shennongjia Group sections in Shennongjia area (Tian et al., 2018). Study localities are marked in (D) with red stars: 1, Jiulongwan (30° 48' 15.648" N, 111° 03' 18.998" E, 704 m elevation); 2, Huajipo (30° 46' 55.692" N 111° 02' 01.747" E, 549 m elevation). (C–D) are adapted from Ye et al. (2019).

with diagenetic fluids than clast interior.

2. Geological setting

The depositional age of the Nantuo Formation is constrained by zircon U-Pb dates from tuffaceous layers below, within, and above the formation. Its minimum age is constrained by a 634.57 ± 0.88 Ma tuffaceous layer in the topmost part of the formation at the E'shan section (see Fig. 1C for locality) in Yunnan Province (Zhou et al., 2019), and a 635.2 ± 0.6 Ma tuffaceous layer from the overlying cap dolostone of the Doushantuo Formation cap dolostone at the Wuhe-Gaojiaxi section (see Fig. 1D for locality) in the Yangtze Gorges (Condon et al., 2005). A tuffaceous layer from the Datangpo Formation immediately below the Nantuo Formation (see Fig. 2A for the spatial distribution of the Datangpo Formation in the Yangtze Craton) yielded an age of 654.5 ± 3.8 Ma at Maopingdong (see Fig. 1C for locality) in Hunan Province, where another tuffaceous bed near the base of the Nantuo Formation yielded a 636 ± 4.9 Ma age (Zhang et al., 2008). These dates constrain deposition of the Nantuo Formation to the late Cryogenian, during the Marinoan Snowball Earth glaciation (Hoffman et al., 2017). Trace element data suggest that at some locations the Nantuo Formation was deposited under an anoxic and possibly ferruginous water column (Gu et al., 2019). Additionally, thin black shale intervals from the Nantuo Formation in the Shennongjia area contain macroalgal fossils (Bykova et al., 2020; Ye et al., 2015), suggesting the presence of open waters with an active biosphere when these sediments were deposited.

The Nantuo Formation thickens basinward to the southeast in Guangxi Province, reaching a maximum thickness of ~ 2000 m, whereas updip on the paleoshelf areas (e.g., Huangling Anticline, see Fig. 1D for locality), it measures less than 100 m and is absent in some areas (see Fig. 2A for a general stratigraphic profile of the Yangtze Platform) (Jiang et al., 2011; Zhang et al., 2011). In the study area of the Yangtze Gorges (red stars in Fig. 1D, red text "YGA" Fig. 2A), the Nantuo Formation is ~ 80 m thick (Hu et al., 2012a; Lang et al., 2018).

In the Yangtze Gorges area (see Fig. 1D for locality), the Nantuo Formation unconformably overlies quartz arenites of the Tonian Liantuo Formation, the Tonian Huangling granite, or Archean gneisses (Zhao et al., 2013a; Zhao et al., 2013b). Earlier Cryogenian strata are missing in this region, but they become progressively more complete to the south (e.g., the Datangpo/Xiangmeng Formation at Changyang, see Fig. 1D for

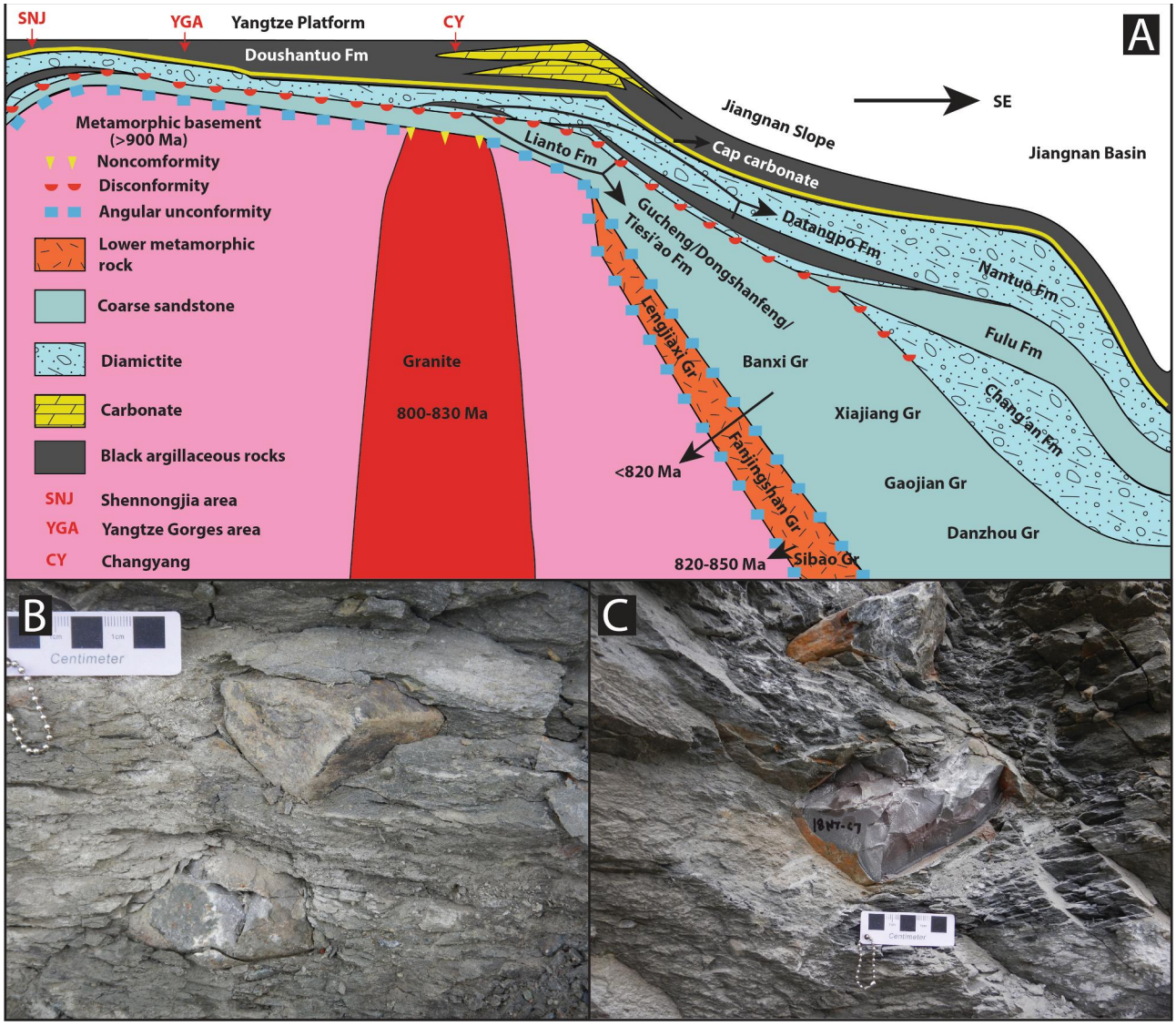

Fig. 2. Simplified Tonian-Ediacaran stratigraphic architecture in South China (A) and field photographs of representative faceted carbonate clasts in the Nantuo Formation at the Huajipo section in the Yangtze Gorges area (B-C). (A) Generalized stratigraphic profile of the Yangtze Platfrom from shallow facies (central-left) to deeper basinal facies (far left and right). Adapted from Xiao et al. (2014). (B-C) Faceted clasts in Nantuo diamictite. Clast shown in (C) above the scale bar is clast 7 (sample 18NT-C7) analyzed in this study. Scale bar in centimeters.

locality and Fig. 2A for a generalized regional stratigraphic profile) (Lu et al., 1985; Zhang et al., 2011) and in the Shennongjia area to the northwest (Chen et al., 2021; Kuang et al., 2022). Across the Yangtze Craton, the Nantuo Formation is overlain by the basal Ediacaran cap dolostone of the Doushantuo Formation (Jiang et al., 2011; Liu et al., 2014).

Previous studies of the sedimentary provenance of the Nantuo Formation have focused on detrital zircon analysis. Cui et al. (2014) presented detrital zircon populations dating to 635 ± 8 Ma, 631 ± 9 Ma, 2192 ± 22 Ma, 2458 ± 14 Ma, and 2496 ± 18 Ma, whereas Zhao et al. (2018) reported detrital zircon age populations dating to 800–820 Ma, 1940–1960 Ma, 2560–2600 Ma, and 2900–3000 Ma. Ye et al. (2019) suggested that detrital zircon age populations of 875 ± 14 Ma, 1880 ± 30 Ma, and 2883 ± 140 Ma were derived from Tonian Huangling granite, Paleoproterozoic metamorphic rocks, and Archean gneisses in the Yangtze Craton, respectively.

3. Materials and methods

We collected 18 carbonate clasts (identified by effervescence with diluted HCl acid) from the Nantuo Formation at two roadcuts in the Yangtze Gorges area in 2018 (Fig. 1D, 2B-C): 12 clasts from the Huajipo section (30° 46′ 55.692″ N, 111° 02′ 01.747″ E; sample numbers 18NT-C1 to 18NT-C12), and six clasts (sample numbers 18NT-C12.5 to 18NT-C17) as well as a sample of Nantuo diamictite matrix (sample number JLW-NT-M1) from the Jiulongwan section (30° 48′ 15.648″ N, 111° 03′ 18.998″ E) respectively. Nantuo diamictites in the Yangtze Gorges area are interpreted as deposits in a glacial littoral environment (Lang et al., 2018).

We prepared polished slabs and petrographic thin sections of the clasts (Figs. 3–6), which were examined and photographed under reflected and transmitted light microscopes. Limestone or dolostone composition was determined using alizarin red staining. We sampled

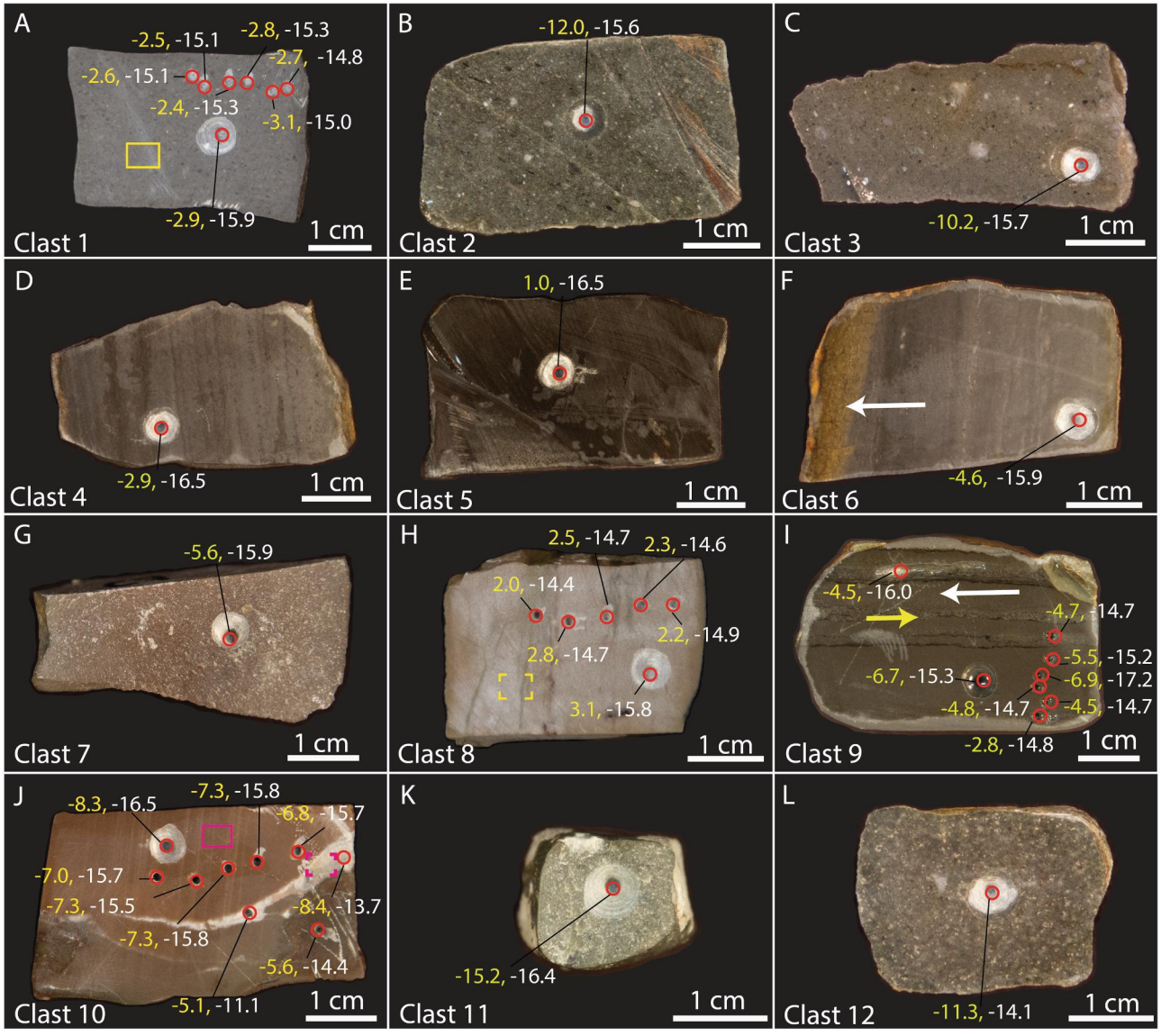

Fig. 3. Reflected light photographs of polished slabs of Nantuo carbonate clasts from the Huajipo section. $\delta^{13}C$ values in yellow and $\delta^{18}O$ values in white. (A) Clast 1, lime wackestone. (B) Clast 2, dolomitic wackestone. (C) Clast 3, angular calcareous quartz arenite. (D) Clast 4, laminated micrite clast. (E) Clast 5, laminated micrite. (F) Clast 6, clast of laminated micrite with a rim of iron oxide (possibly derived from recent oxidation of pyrite) on the left side (arrow), which was oriented downwards within the diamictite matrix. (G) Clast 7, laminated micrite clast. (H) Clast 8, laminated micrite. (I) Clast 9, rounded clast of laminated silty lime wackestone with fine-grained layers (white arrow) and coarse-grained layers (yellow arrow). (J) Clast 10, laminated micrite with calcite veins. (K) Clast 11, rounded and faceted clast of micrite. (L) Clast 12, rounded clast of lime wackestone. Rectangles or frames in (A), (H), and (J) mark general areas from which corresponding thin section images shown in Fig. 4A, 4G, and 4 J–K were taken.

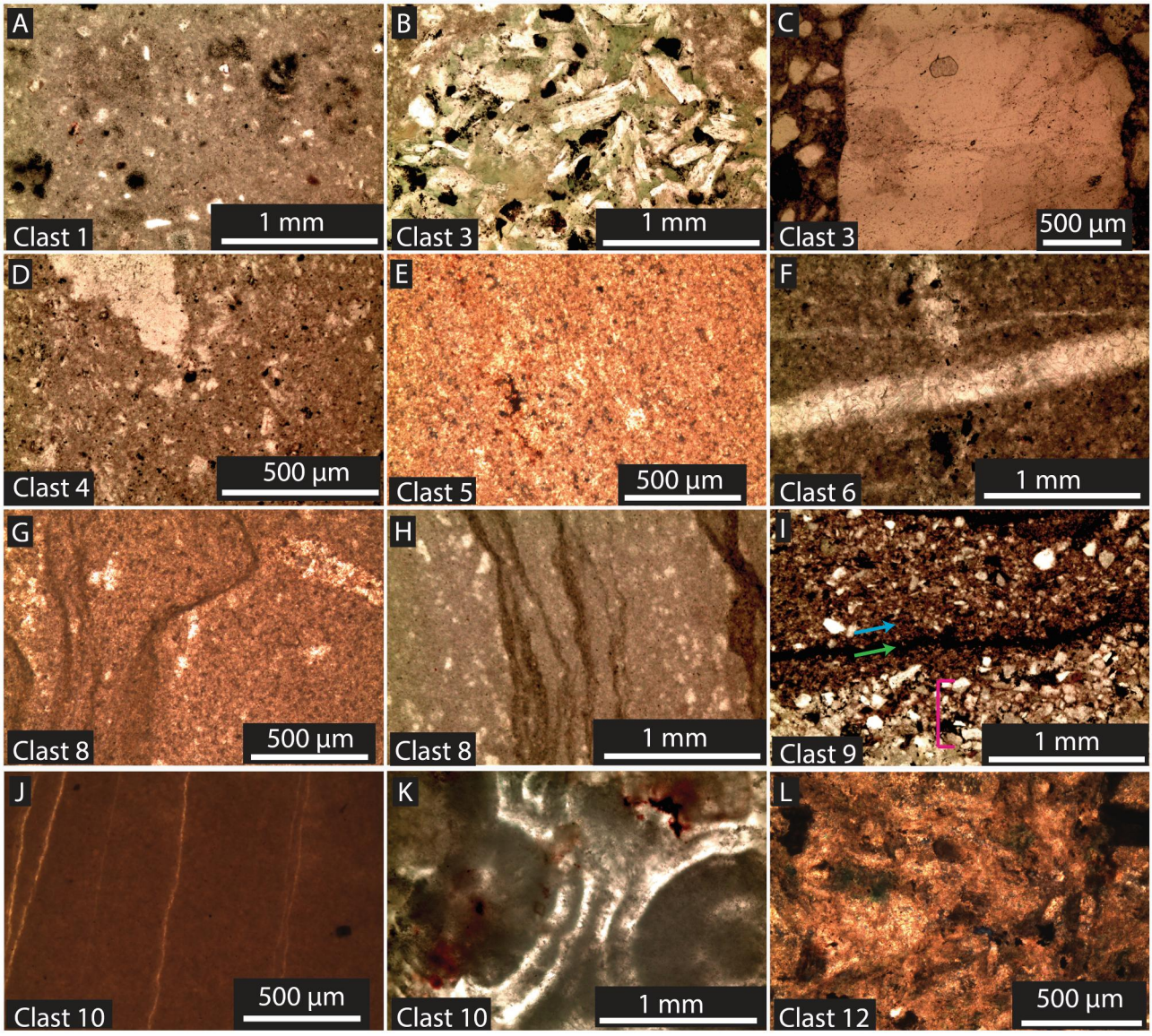

Fig. 4. Plane-polarized transmitted light photomicrographs of petrographic thin sections showing microtextures of Nantuo carbonate clasts from the Huajipo section. (A) Lime wackestone with quartz and lithic grains, from area marked by yellow rectangle in Fig. 3A. (B) Clast 3, lathe-shaped grains and chloritized matrix. (C) Clast 3, calcareous quartz arenite with poorly sorted grains. (D) Clast 4, poorly sorted, angular grains in a carbonate matrix. (E) Clast 5, locally sparry texture in a dominantly micritic clast. (F) Clast 6, finely laminated micrite with veins in multiple orientations. (G) Clast 8, irregular laminations. (H) Clast 8, laminated micrite, from area marked by yellow frame in Fig. 3H. These laminae are accentuated by pressure solution during burial. (I) Clast 9, silty lime wackestone with coarser grains (maroon bracket), fine laminae (green arrow), and finer grains (blue arrow). (J) Clast 10, laminated micrite with locally homogenous matrix and calcite veins, from area marked by maroon rectangle in Fig. 3J. (K) Clast 10, vein-infilling botryoidal calcite cement, from area marked by maroon frame in Fig. 3J. (L) Clast 12, with diffuse grain boundaries.

powders from the polished slabs for $\delta^{13}C$ and $\delta^{18}O$ analysis, using a Dremel tool with a 1.5 mm drill bit or a Servo 7150 microdrill press with a 0.6 mm drill bit. Most clasts were microsampled using the Dremel tool, but six clasts (i.e., clast 1, 8–10, 13, 17 illustrated in Fig. 3A, 3H–J, 5B, 5F, respectively) were drilled using the microdrill press to achieve greater spatial resolution in order to (1) target specific fabrics or (2) acquire transects across clasts to test whether there are interior-exterior gradients related to post-reworking alteration (Table 1).

We measured $\delta^{18}O$ and $\delta^{13}C$ values on an Isoprime 100 Isotope Ratio Mass Spectrometer (IRMS) coupled to a MultiFlowGEO headspace analyzer. For each analysis, we weighed 0.4–0.8 mg of powder into a septum-sealed glass vial. We used the headspace analyzer to evacuate the vial with helium before reacting overnight with glacial phosphoric acid at 70 °C to fully dissolve the carbonate. The evolved CO_2 gas was then analyzed on the IRMS. We normalized the $\delta^{13}C$ and $\delta^{18}O$ values to the Vienna PeeDee Belemnite (VPDB) scale using IAEA-CO-1 ($\delta^{13}C$ = 2.492 ‰ ± 0.030 ‰, $\delta^{18}O$ = –2.4 ‰ ± 0.1 ‰) and NIST NBS-18 ($\delta^{13}C$ = –5.014 ‰ ± 0.035 ‰, $\delta^{18}O$ = –23.2 ‰ ± 0.1 ‰) standards analyzed in runs with our samples via two-point linear normalization. We calculated uncertainty (1σ) to be ± 0.3 ‰ for $\delta^{13}C$ and ± 0.2 ‰ for $\delta^{18}O$ following Szpak et al. (2017).

To determine if the Nantuo carbonate clasts presented here have statistically different isotopic values from each other, we conducted one-way ANOVA analyses of isotopic data from clasts with replicate analyses (i.e., the six clasts analyzed for interior-exterior transects). If statistical difference was found, we further analyzed the data using a Tukey's Honestly Significant Difference post-hoc test for each pair-wise comparison. Similarly, we conducted a one-way ANOVA analysis to determine whether the 17 Nantuo clasts analyzed in this study have statistically different isotopic values from the Shennongjia Group

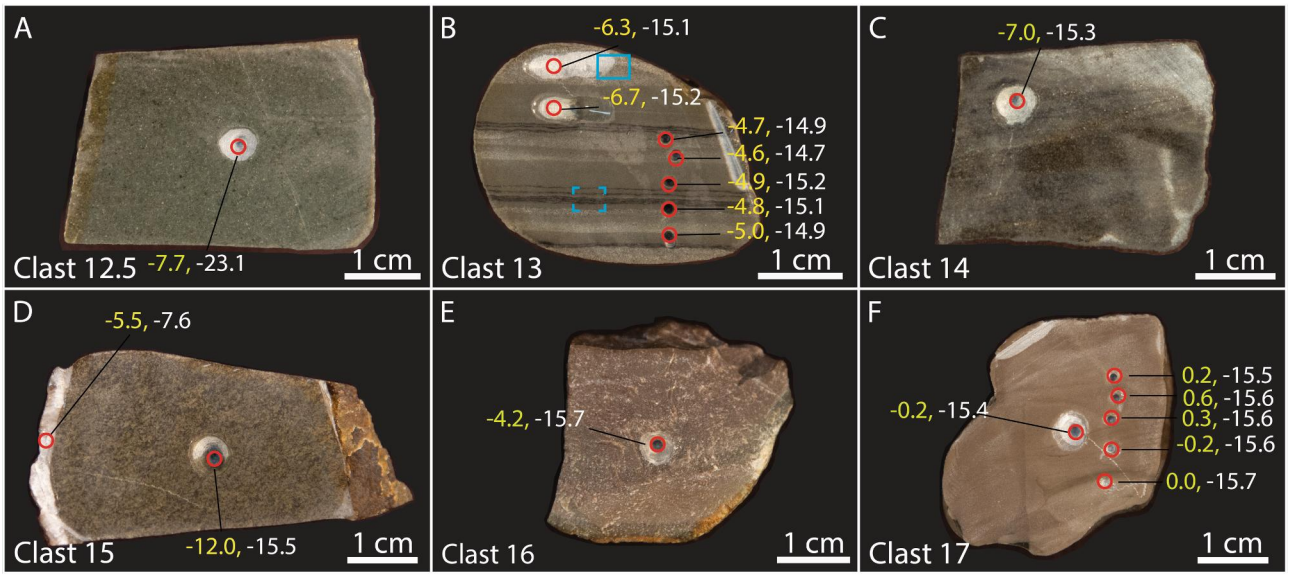

Fig. 5. Reflected light photographs of polished slabs of Nantuo carbonate clasts from the Jiulongwan section with stable isotope values. $\delta^{13}C$ values in yellow and $\delta^{18}O$ values in white. (A) Clast 12.5, faceted dolomitic wackestone clast. (B) Clast 13, laminated micrite with laminations of coarse calcareous grains and fine dolomitic grains. (C) Clast 14, silty calcareous wakestone clast. (D) Clast 15, dolomitic packstone clast. (E) Clast 16, angular clast of pink laminated micrite. (F) Clast 17, an irregularly shaped clast of laminated micrite. Rectangle and frame in (B) mark general areas from which corresponding thin section images shown in Fig. 6A and 6B were taken.

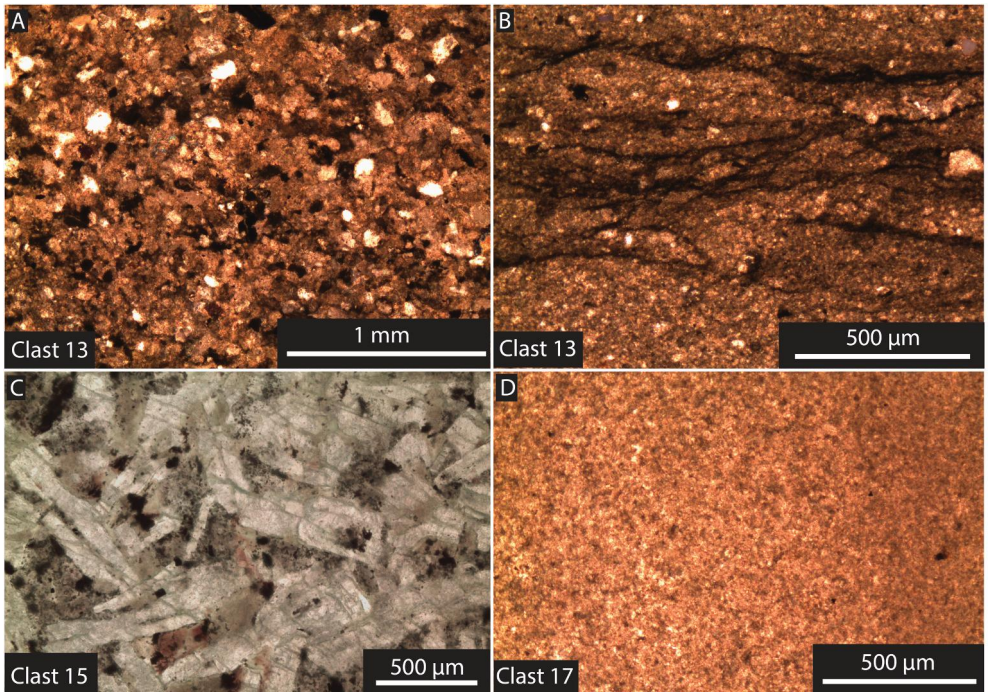

Fig. 6. Transmitted light photomicrographs of thin sections showing microtextures of Nantuo carbonate clasts from the Jiulongwan section. (A) Lamina of coarse calcareous grains, from area marked by blue rectangle in Fig. 5 B. (B) Thin laminae of fine dolomitic grains from area marked by blue bracket frame in Fig. 5B. (C) Clast 15, crystalline dolomite with large, lathe-like crystals. (D) Clast 17, laminated micrite with locally homogenous microtexture.

carbonates; for this analysis, the $\delta^{13}C$ and $\delta^{18}O$ data were tested separately, with pooled Nantuo clast data (n = 53) compared with pooled Shennongjia Group data from the literature (n = 911 from Tian et al., 2018, n = 126 from Zou et al., 2019). Additionally, we carried out a bootstrap analysis to test whether the Nantuo carbonate clasts and Shennongjia Group carbonates have similar $\delta^{13}C$ and $\delta^{18}O$ values; in this analysis, $\delta^{13}C$ and $\delta^{18}O$ pairs were resampled with replacement to reproduce the original Nantuo and Shennongjia sample sizes, the mean was calculated for each resampled population, and this was repeated 5000 times to generate the 95% and 99% confidence intervals.

4. Results

4.1. Petrology/lithology

The clasts are limestone (n = 15) or dolomitic mudstones/

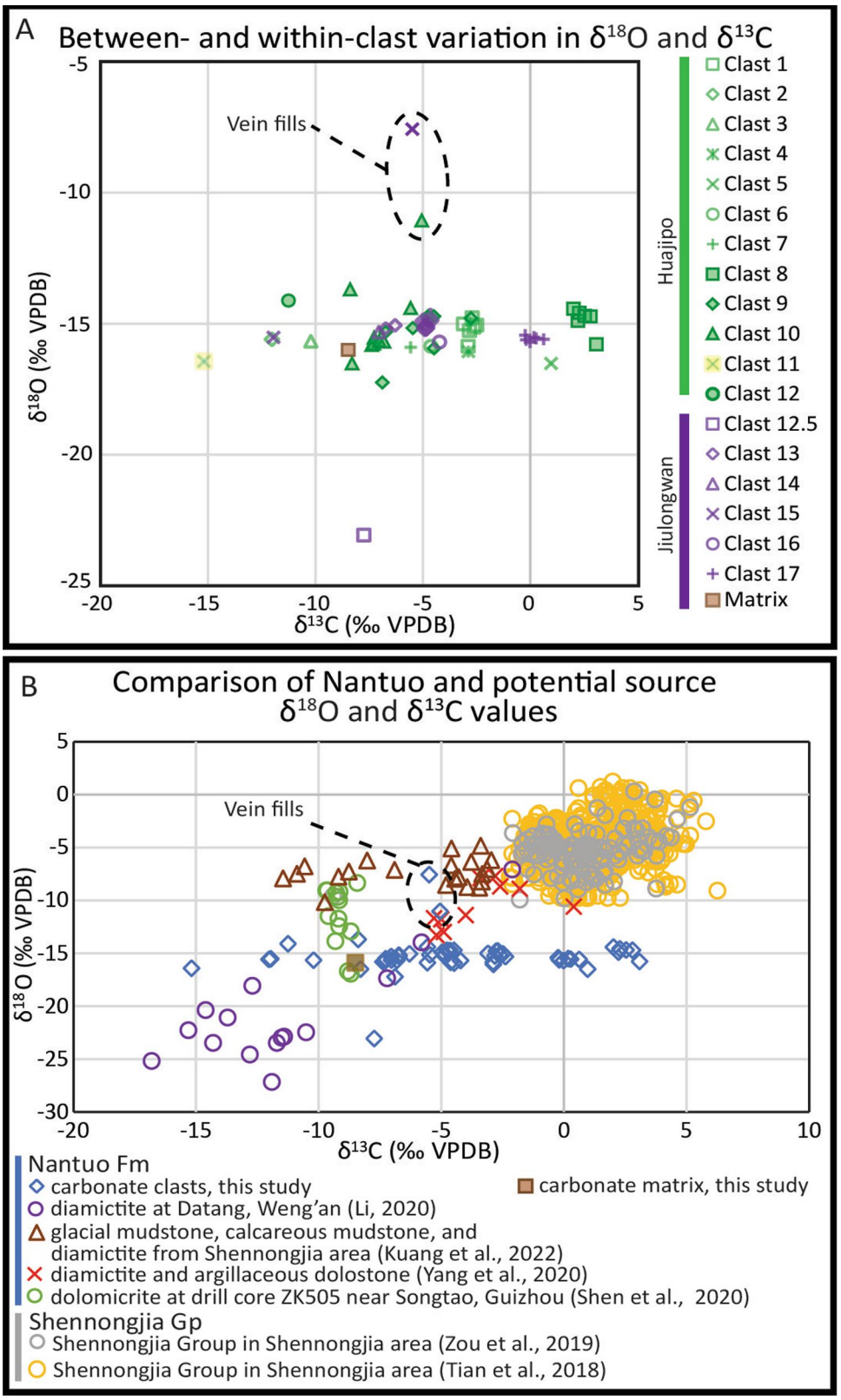

Fig. 7. $\delta^{13}C$ and $\delta^{18}O$ of carbonate clasts in Nantuo Formation (this study), calcareous matrix in Nantuo diamictite (Li, 2020; Kuang et al., 2022; Yang et al., 2020), bedded carbonates in the Nantuo Formation (Shen et al., 2020), and carbonate of the Mesoproterozoic Shennongjia Group (Tian et al., 2018; Zou et al., 2019). (A) $\delta^{13}C$ and $\delta^{18}O$ values of Nantuo carbonate clasts and diamictite matrix analyzed in this study. (B) $\delta^{13}C$ and $\delta^{18}O$ of Nantuo carbonate clasts and diamictitie matrix from this study compared with published data from the Nantuo Formation and the Shennongjia Group carbonates. Analytical errors smaller than symbol size.

wackestones (n = 3) in lithological composition. Detrital components in wackestone clasts are dominated by quartz and lithic grains. Grain sizes range from very coarse (Fig. 4C and 4D) to silt sized (Fig. 3E). Pyrite (Fig. 4A) and chlorite (Fig. 4B) occur in some clasts. Some clasts contain post-depositional fabrics, including calcite veins (Fig. 4F, 4 J) and cracks filled with blocky and botryoidal cements (Fig. 4K). Others exhibit homogenous textures (Fig. 4E and 6D). Sedimentary laminae, when present, tend to be wavy and uneven, likely accentuated by pressure solution during burial (e.g., Fig. 4G, 4H. and 6B). Two clasts contain interbedded coarse and finer grains (Fig. 3I, 4I, 5B, 6A, and 6B).

Table 1
$\delta^{13}C$ and $\delta^{18}O$ data from carbonate clasts and diamictite matrix of the Cryogenian Nantuo Formation. Samples 18NT-C1 to 18NT-C12 are from the Huajipo section. Samples 18NT-C12.5 to 18NT-C17 and sample JLW-NT-M1 are from the Jiulongwan section.

Sample #	lithology	Sampling method	$\delta^{13}C$ (‰ VPDB)	Within-clast statistics	$\delta^{18}O$ (‰ VPDB)	Within-clast statistics
Measurements of clasts						
18NT-C1	Lime wackestone	Dremel tool	–2.9	range: –3.1 to –2.4	–15.9	range: –15.9 to
		Press drill	–2.7	mean: –2.7	–14.8	–14.8
			–3.1	s.d.: 0.2	–15.0	mean: –15.2
			–2.8		–15.3	s.d.: 0.3
			–2.4		–15.3	
			–2.5		–15.1	
			–2.6		–15.1	
18NT-C2	Dolomitic wackestone	Dremel tool	–12.0		–15.6	
18NT-C3	Calcareous quartz arenite	Dremel tool	–10.2		–15.7	
18NT-C4	Laminated micrite	Dremel tool	–2.9		–16.1	
18NT-C5	Laminated micrite	Dremel tool	1.0		–16.5	
18NT-C6	Laminated micrite	Dremel tool	–4.6		–15.9	
18NT-C7	Micrite	Dremel tool	–5.6		–15.9	
18NT-C8	Laminated micrite	Dremel tool	3.1	range: 2.0 to 3.1	–15.8	range: –15.8 to
		Press drill	2.2	mean: 2.5	–14.9	–14.4
			2.3	s.d.: 0.4	–14.6	mean: –14.9
			2.5		–14.7	s.d.: 0.5
			2.8		–14.7	
			2.0		–14.4	
18NT-C9	Laminated silty lime wackestone	Dremel tool	–6.7	range: –6.9 to –2.8	–15.3	range: –17.2 to
			–4.5	mean: –5.0	–15.9	–14.7
		Press drill	–2.8	s.d.: 1.3	–14.8	mean: –15.3
			–4.5		–14.7	s.d.: 0.9
			–4.8		–14.7	
			–6.9		–17.2	
			–5.5		–15.2	
			–4.7		–14.7	
18NT-C10	Laminated micrite	Dremel tool	–8.3	range: –8.3 to –5.6	–16.5	range: –16.5 to
		Press drill	–6.8	mean: –7.1	–15.7	–14.4
			–7.3	s.d.: 0.8	–15.8	mean: –15.6
			–7.4		–15.8	s.d.: 0.6
			–7.3		–15.5	
			–7.0		–15.7	
			–5.6		–14.4	
18NT-C11	Micrite	Dremel tool	–15.2		–16.4	
18NT-C12	Lime wackestone	Dremel tool	–11.3		–14.1	
18NT-C12.5	Dolomitic wackestone	Dremel tool	–7.7		–23.1	
18NT-C13	Laminated micrite with calcareous coarse grains and dolomitic finer grains	Dremel tool	–6.3	range: –6.7 to –4.6	–15.1	range: –15.2 to
			–6.7	mean: –5.3	–15.2	–14.7
		Press drill	–5.0	s.d.; 0.9	–14.9	mean: –15.0
			–4.8		–15.1	s.d.: 0.2
			–4.9		–15.2	
			–4.6		–14.7	
			–4.7		–14.9	
18NT-C14	Silty calcareous wackestone	Dremel tool	–7.0		–15.3	
18NT-C15	Dolomitic packstone	Dremel tool	–12.0		–15.5	
18NT-C16	Laminated micrite	Dremel tool	–4.2		–15.7	
18NT-C17	Laminated micrite	Dremel tool	–0.2	range: –0.2 to 0.6	–15.4	range: –15.7 to
		Press drill	0.0	mean: 0.1	–15.7	–15.4
			–0.2	s.d.: 0.3	–15.6	mean: –15.6
			0.3		–15.6	s.d.: 0.1
			0.6		–15.6	
			0.2		–15.5	
All-clast statistics			range: –15.2 to 3.1; mean: –4.2; s.d.: 4.1		range: –23.1 to –14.1; mean: –15.5; s.d.: 1.2	
Other Measurements						
18NT-C10	Calcitic vein	Dremel tool	–8.4		–13.7	
		Press drill	–5.1		–11.1	
18NT-C15	Calcitic vein	Dremel tool	–5.5		–7.6	
JLW-NT-M1	Diamictite matrix	Dremel tool	–8.5		–15.9	

4.2. Isotopic compositions

We analyzed the isotopic compositions of clasts and fine-scale textural features within clasts (Table 1). The $\delta^{18}O$ values range from –23.1 ‰ to –13.5 ‰ with the majority of the values between –17.3 ‰ to –13.5 ‰. Only a handful of samples fall outside this range: a sample from clast 12.5 (–23.1 ‰, Fig. 5A), a vein-filling carbonate sample from clast 10 (–11.1 ‰, Fig. 3J), and a vein-filling carbonate sample on an exterior surface of clast 15 (–7.6 ‰, Fig. 6D). The $\delta^{13}C$ values for all clasts range from –15.2 ‰ to + 3.1 ‰. For a subset of clasts with multiple measurements (n = 6), we performed a one-way ANOVA test to evaluate whether clasts had statistically different isotopic values from one another (Supplemental Table S1). We found significant differences among $\delta^{13}C$ values of the clasts, but not among the $\delta^{18}O$ values. We then

evaluated the $\delta^{13}C$ values of the clasts in all possible pairwise comparisons via a Tukey's Honestly Significant Difference post-hoc test. This showed that the $\delta^{13}C$ values were significantly different in all pairwise comparisons, except between clasts 9 and 13 (Supplemental Table S2).

Within-clast ranges of isotopic values are + 0.7 ‰ to + 4.1 ‰ (mean = 1.9 ‰) for $\delta^{13}C$ and 0.3 ‰ to 2.5 ‰ (mean = 1.3 ‰) for $\delta^{18}O$ (Table 1). The exterior-interior transects of six clasts do not show significant mm-scale spatial variation in the isotope values. The sample of diamictite matrix yielded a $\delta^{13}C$ value of –8.5 ‰ and a $\delta^{18}O$ value of –15.9 ‰.

We compared the $\delta^{13}C$ and $\delta^{18}O$ values between the Nantuo carbonate clasts (n = 53 measurements) and carbonate materials of the Shennongjia Group (n = 911 from Tian et al., 2018; n = 126 from Zou et al., 2019) via one-way ANOVA analysis, which showed that the Nantuo clasts have statistically different $\delta^{13}C$ and $\delta^{18}O$ values from the Shennongjia group material (Supplemental Table S3). Bootstrap analysis also showed that the Nantuo carbonate clasts and Shennongjia Group carbonates are distinct in the $\delta^{13}C$–$\delta^{18}O$ space (Fig. 8).

5. Discussion

5.1. Post-reworking alteration and comparison with previously published data from the Nantuo Formation

$\delta^{13}C$ and $\delta^{18}O$ values of carbonate materials have been used to evaluate the provenance of transported sedimentary material (Trower and Grotzinger, 2010). When using $\delta^{13}C$ and $\delta^{18}O$ values of carbonate clasts to constrain provenance, it is important to assess whether the isotopic signatures of the sediments (e.g., the Nantuo carbonate clasts) were altered after reworking. For example, post-reworking alteration could have occurred due to chemical weathering of the clasts during transportation or due to diagenetic alteration after the clasts were redeposited. Such alteration can be tested by examining the interior-exterior transects of Nantuo carbonate clasts, because alteration would affect the exterior more than the interior of clasts, as can be seen in the weathering rinds of weathered clasts. However, the Nantuo clasts show no exterior-interior gradients in $\delta^{13}C$ or $\delta^{18}O$ (Table 1; Fig. 7A). Thus, the $\delta^{13}C$ and $\delta^{18}O$ values of the Nantuo clasts do not seem to have suffered significant post-reworking alteration.

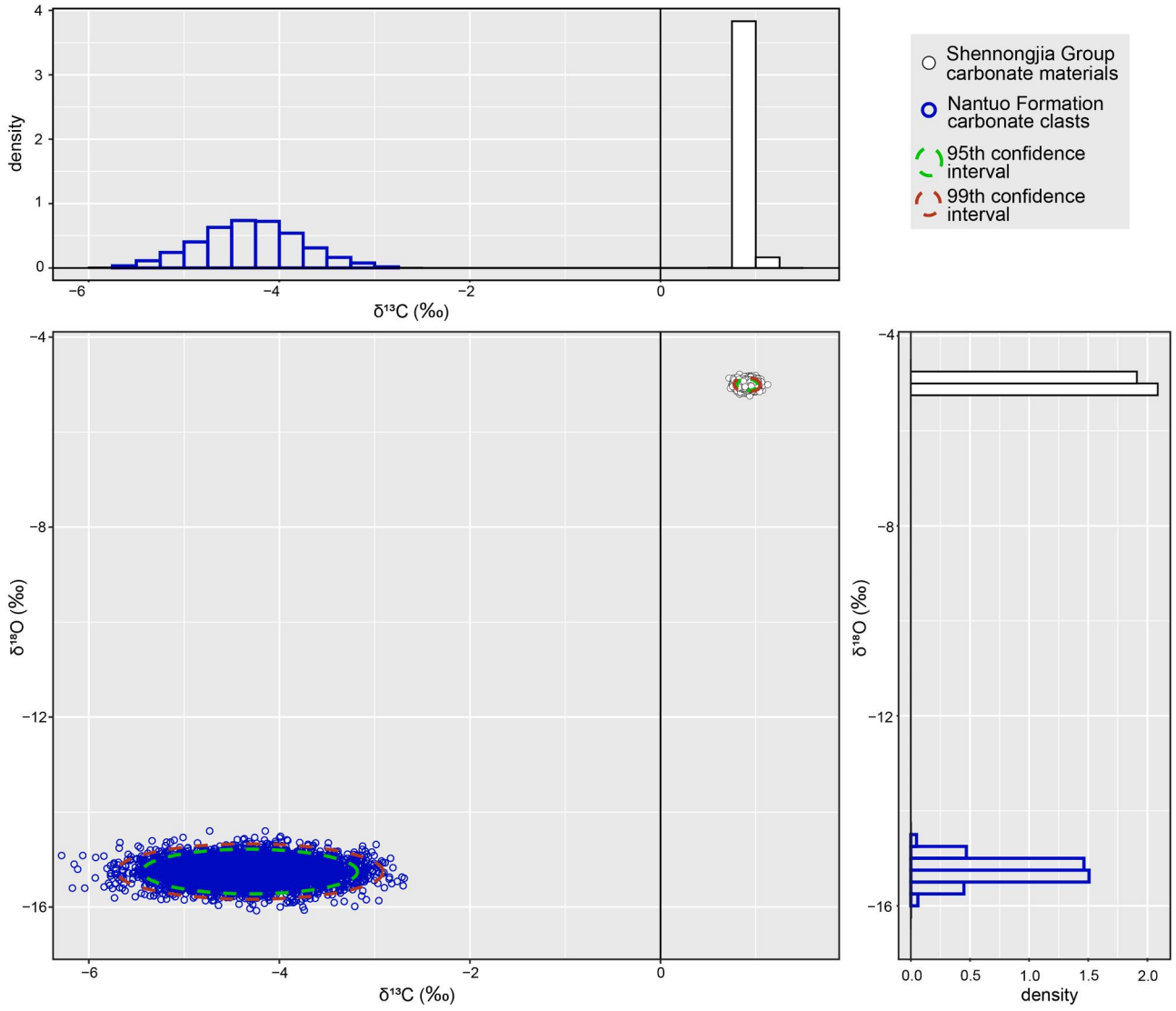

Fig. 8. Result of bootstrap analysis $\delta^{13}C$–$\delta^{18}O$ values of Nantuo carbonate clasts (this study) and Shennongjia Group carbonates (Tian et al., 2018; Zou et al., 2019). The $\delta^{13}C$–$\delta^{18}O$ data pairs were randomly resampled with replacement to reproduce the original sample sizes. A total of 5000 iterations were performed and the mean $\delta^{13}C$ ans $\delta^{18}O$ values of each iteration was recorded to produce the histograms and cross-plots. The green and red dashed ellipses represent the 95% and 99% confidence intervals for the resampled data. The histogram bar plots are binned in 0.25 ‰ segments.

The very low $\delta^{18}O$ values (ca. –15 ‰) of the Nantuo carbonate clasts could be taken as evidence for diagenetic alteration, but we argue such alteration likely occurred before reworking. Kaufman et al. (2007) regarded Precambrian carbonate $\delta^{18}O$ values lower than –10 ‰ and Veizer et al. (1999) suggested Phanerozoic carbonate $\delta^{18}O$ values lower than –8 ‰ may have been diagenetically altered. However, as discussed above, the lack of an exterior-interior gradient in $\delta^{18}O$ values (and in $\delta^{13}C$ values) argues against post-reworking alteration, and it is likely that alteration occurred before clast reworking, in which case the $\delta^{18}O$ and $\delta^{13}C$ values can still be used to track provenance. Also, considering that pre-Cryogenian seawaters likely had lower $\delta^{18}O$ (Galili et al., 2019) and higher temperatures (Robert and Chaussidon, 2006) relative to modern seawaters, it is possible that the $\delta^{18}O$ values of the Nantuo carbonate clasts may reflect the primary depositional signatures. Furthermore, considering that $\delta^{18}O$ is more susceptible to alteration than $\delta^{13}C$ during interaction with diagenetic, hydrothermal, or meteoric fluids (Banner and Hanson, 1990; Corsetti and Kaufman, 2003; Jacobsen and Kaufman, 1999), alteration tends to lead to more variable $\delta^{18}O$ values and less variable $\delta^{13}C$ values, unless the system is completely fluid buffered with regard to $\delta^{18}O$ but not so with regard to $\delta^{13}C$. Yet the Nantuo clasts have remarkably consistent $\delta^{18}O$ values (Fig. 7A), whereas their $\delta^{13}C$ values are variable. Thus, the Nantuo clasts likely preserve the $\delta^{13}C$ and $\delta^{18}O$ values of their provenance, although at this point, we cannot rule out the possibility that the $\delta^{18}O$ values of the Nantuo clasts may have been completely reset to uniform values around –15 ‰ due to post-reworking interaction with glacial melt water in a fluid-buffered regime, whereas their $\delta^{13}C$ values were minimally or partially reset and thus remain more variable.

Post-reworking alteration of $\delta^{13}C$ and $\delta^{18}O$ values of the Nantuo carbonate clasts can be further evaluated by a comparison with the isotopic values of other carbonate components in the Nantuo Formation of South China (Fig. 7B). Published geochemical data of Nantuo carbonate material from other sections show $\delta^{13}C$ overlapping with and $\delta^{18}O$ more variable than the clast data reported here (Fig. 7B). Li (2020) reported isotopic values of calcareous matrix in Nantuo Formation diamictite at the Datang section in the Weng'an area (see Fig. 1C for locality). This matrix has $\delta^{13}C$ values that overlap with the range of data reported here, and $\delta^{18}O$ values that are more negative (average: –20.9 ‰) and vary over a broader range (–27.2 to –7.1 ‰). Long (2016) and Shen et al. (2020) reported on a 1.5 m-thick dolomicrite bed that occurs locally in the Nantuo Formation at two drill cores in the Songtao area of Guizhou Province (see Fig. 1C for locality). Again, their $\delta^{13}C$ values (–9.7 to –8.4 ‰) overlap with the data reported here but have a narrower range, and their $\delta^{18}O$ values (–17.0 to –8.4 ‰) are wider ranging than the clasts in this study. Kuang et al. (2022) report $\delta^{13}C$ and $\delta^{18}O$ values from Nantuo Formation glacial mudstones, diamictites, and a calcareous mudstone from four localities in the Shennongjia area. This Nantuo Formation material analyzed by Kuang et al. (2022) is isotopically more enriched in ^{18}O than carbonate clasts reported here, but the $\delta^{13}C$ values are within the range reported here. Finally, Yang et al. (2020) reported isotopic values of Nantuo diamictites and argillaceous dolostones in the Shennongjia area (see Fig. 1D for locality). Their $\delta^{13}C$ values range from –5.3 to + 0.4 ‰, which is within the range of $\delta^{13}C$ data in this study, but their $\delta^{18}O$ values range from –13.3 to –7.3 ‰, higher than the values reported in this study.

Several factors may have contributed to the differences among isotopic data reported in this and earlier studies. First, the previously published data came from localities outside the Yangtze Gorges area, and there may have been regional variation in $\delta^{18}O$ and $\delta^{13}C$. Second, some of these previous studies analyzed bedded dolomicrite and argillaceous dolostone in the Nantuo Formation, (e.g., Long, 2016; Shen et al., 2020; Yang et al., 2020), which are not detrital in origin and thus may not have the same isotopic compositions as the Nantuo clasts. Finally, Nantuo diamictite matrix from previous studies may contain carbonate cement and detrital rock flour. Carbonate cement would be distinct from Nantuo carbonate clasts in isotopic signatures, whereas carbonate rock flour is expected to be similar to Nantuo carbonate clasts in isotopic signatures, although it is more susceptible to post-reworking diagenetic alteration because of its finer grain size. Indeed, Li (2020) and Yang et al. (2020) argued that variable $\delta^{18}O$ values from the diamictite, bedded dolomicrite, and argillaceous dolostone of the Nantuo Formation were likely overprinted by diagenesis. The Nantuo carbonate clasts, however, have more consistent $\delta^{18}O$ values, indicating that they suffered a lesser degree of post-reworking alteration than the diamictite matrix.

5.2. *Provenance of Nantuo carbonate clasts*

Considering the Nantuo clasts analyzed in this study likely preserve their pre-reworking isotopic signatures, we can use the $\delta^{13}C$ and $\delta^{18}O$ data to test the hypothesis that Nantuo carbonate clasts were derived exclusively from Mesoproterozoic carbonate rocks of the Shennongjia Group, the only major extant pre-Marinoan carbonates in South China (Zou et al., 2019). The $\delta^{13}C$–$\delta^{18}O$ values of Nantuo carbonate clasts do not overlap with those reported from the Shennongjia Group (Fig. 7B), which have $\delta^{13}C$ values ranging from –9.4 to + 6.27 ‰ and $\delta^{18}O$ values from –10.0 to + 1.2 ‰ (Zou et al., 2019; Tian et al., 2018). This assessment is further confirmed by ANOVA and bootstrap analyses, showing that the Shennongjia Group and Nantuo carbonate clasts are distinct in $\delta^{13}C$ and $\delta^{18}O$ values (Supplemental Table S3, Fig. 8). It is also consistent with largely different $\delta^{13}C$ and $\delta^{18}O$ values between the Shennongjia Group and all calcareous components in the Nantuo Formation (Fig. 7B). Finally, this assessment is supported by the lithological differences between the Shennongjia Group and Nantuo carbonate clasts: Shennongjia Group carbonates are dominated by dolostones (Tian et al., 2018; Zou et al., 2019)— though Tian et al., (2018) did report some limestone units within the Shennongjia Group, whereas the Nantuo carbonate clasts analyzed in this study are primarily limey in composition. We thus falsify the hypothesis that carbonate clasts in the Nantuo Formation in the Three Gorges area were sourced from the Shennongjia Group and the hypothesis that the Shennongjia Group was the only source of carbonate clasts in the Nantuo Formation across the Yangtze Craton.

If the Nantuo carbonate clasts in the Yangtze Gorges area were not sourced from the Shennongjia Group, we hypothesize they came from other pre-Marinoan carbonate successions in South China that have since been eroded. Notably, the Tonian Wujiatai Formation (Kuang et al., 2019), which has rather limited outcrops in the Zhangcunping area of the Huangling anticline (see Fig. 1D for locality) (Hu et al., 2012b) may represent remnants of source strata that supplied carbonate clasts to the Nantuo Formation during the Marinoan glaciation. This can be tested by future investigation of the Wujiatai Formation.

Alternatively, Nantuo carbonate clasts could have been transported from the Indian Craton, which hosts pre-Marinoan carbonates and may have been paleogeographically close to South China during the late Neoproterozoic (Bao et al., 2018). Qi et al. (2018) used detrital zircon data to infer that the South China Craton abutted the Indian Craton during the Ediacaran, with the Cathaysia Block sitting between the Indian Craton and the Yangtze Craton. Jiang et al. (2003), on the other hand, compared the Ediacaran stratigraphic sequences of the Yangtze Craton and the Indian Craton and concluded that they were deposited in a contiguous sedimentary basin. The major pre-Cryogenian carbonate unit in cratonic India is the Proterozoic Vindhyan Supergroup. Intriguingly, the $\delta^{13}C$ and $\delta^{18}O$ values of the Vindhyan Supergroup, particularly those of the Paleoproterozoic Kajrahat Formation in the Son Valley (Gilleaudeau et al., 2018; Kumar et al., 2002), overlap with those of the Nantuo carbonate clasts reported in this paper. However, a Vindhyan source means that the Nantuo clasts would have travelled thousands of kilometers in either paleogeographic reconstruction and would have traversed the Cathaysia Block and the Jiangnan Orogen between India and the Yangtze Craton in the paleogeographic configuration of Qi et al. (2018). Additionally, some detrital zircon analyses (e.g., Wang et al.,

2021) suggest that the Indian Craton and Yangtze Craton may have rifted away from each other by the time when the Nantuo Formation was deposited. Thus, we tentatively favor an intracratonic origin (e.g., a Wujiatai Formation source) for the Nantuo carbonate clasts in the Yangtze Gorges area given that (1) the abundance of the carbonate clasts in the Nantuo Formation increases from the Yangtze Gorges area towards the northern Huangling anticline and the Shennongjia area (Lu and Qu, 1985; Sha et al., 1963; Zhao et al., 2018), (2) other detrital material in the Nantuo Formation was derived from Yangtze Craton material (Hu et al., 2020; Ye et al., 2019), and (3) the carbonate clasts would not have been particularly resistant, and thus are unlikely to survive long-distance transport. Whether Nantuo carbonate clasts in the Shennongjia area and the northern Huangling anticlines were derived from the Shennongjia Group (Lu and Qu, 1985; Sha et al., 1963; Zhao et al., 2018) remains to be tested, but it is safe to conclude that the Shennongjia Group was not the sole source of Nantuo carbonate clasts in South China.

6. Conclusions

Carbonate clasts in the terminal Cryogenian Nantuo Formation in the Yangtze Gorges area of South China exhibit $\delta^{13}C$ and $\delta^{18}O$ values different from carbonates in the Mesoproterozoic Shennongjia Group, the only major pre-Cryogenian carbonate succession that is extant in South China. Based on the isotopic data, we falsify the hypothesis that Nantuo carbonate clasts in the Yangtze Gorges area were derived from the Shennongjia Group. Instead, we suggest these Nantuo carbonate clasts were derived from pre-Cryogenian carbonate rocks in the Yangtze Craton that have since been mostly or completely eroded; this hypothesis implies that pre-Cryogenian carbonates may have been paleogeographically and/or stratigraphically more extensive than extant today, and that Marinoan glaciers were a powerful erosional agent. Alternatively, but less likely, they may have derived from pre-Cryogenian carbonates in the Indian Craton via long-distance transportation by Marinoan glaciers. Regardless, carbonate clasts in the Nantuo Formation of South China were not exclusively derived from the Shennongjia Group, attesting the extensive denudation of diverse source material and the remarkable influence of the Marinoan glaciation.

CRediT authorship contribution statement

Morrison Nolan: Conceptualization, Methodology, Formal analysis, Investigation, Writing – original draft. **Shuhai Xiao:** Conceptualization, Methodology, Formal analysis, Investigation, Writing – revising. **Benjamin Gill:** Methodology, Investigation, Resources. **Rachel Reid:** Methodology, Formal analysis, Investigation, Resources. **Maxwel Schwid:** Investigation.

Declaration of Competing Interest

The authors declare that they have no known competing financial interests or personal relationships that could have appeared to influence the work reported in this paper.

Acknowledgements

We thank the National Science Foundation (EAR-2021207) for funding, Yezi Yang for laboratory assistance, Michelle Stocker for feedback on an earlier version of the manuscript, Qin Ye and Jiasheng Wang for discussion, and special issue editor Zhongwu Lan and two anonymous reviewers for constructive comments.

Appendix A. Supplementary data

Supplementary data to this article can be found online at https://doi.org/10.1016/j.precamres.2022.106734.

References

Banner, J.L., Hanson, G.N., 1990. Calculation of simultaneous isotopic and trace element variations during water-rock interaction with applications to carbonate diagenesis. Geochim. Cosmochim. Acta 54, 3123–3137. https://doi.org/10.1016/0016-7037(90)90128-8.

Bao, X., Zhang, S., Jiang, G., Wu, H., Li, H., Wang, X., An, Z., Yang, T., 2018. Cyclostratigraphic constraints on the duration of the Datangpo Formation and the onset age of the Nantuo (Marinoan) glaciation in South China. Earth Planet. Sci. Lett. 483, 52–63. https://doi.org/10.1016/j.epsl.2017.12.001.

Bykova, N., LoDuca, S.T., Ye, Q., Marusin, V., Grazhdankin, D., Xiao, S., 2020. Seaweeds through time: Morphological and ecological analysis of Proterozoic and early Paleozoic benthic macroalgae. Precambr. Res. 350, 105875 https://doi.org/10.1016/0016-7037(90)90128-810.1016/j.precamres.2020.105875.

Chen, X., Kuang, H., Liu, Y., Le Heron, D.P., Wang, Y., Peng, N., Wang, Z., Zhong, Q., Yu, H., Chen, J., 2021. Revisiting the Nantuo Formation in Shennongjia, South China: A new depositional model and multiple glacial cycles in the Cryogenian. Precambr. Res. 356, 106132 https://doi.org/10.1016/0016-7037(90)90128-810.1016/j.precamres.2021.106132.

Condon, D., Zhu, M., Bowring, S., Wang, W., Yang, A., Jin, Y., 2005. U-Pb ages from the neoproterozoic Doushantuo Formation, China. Science 308, 95–98. https://doi.org/10.1016/0016-7037(90)90128-810.1144/jgs2016-142.

Corsetti, F.A., Kaufman, A.J., 2003. Stratigraphic investigations of carbon isotope anomalies and Neoproterozoic ice ages in Death Valley, California. GSA Bulletin 115, 916–932. https://doi.org/10.1016/0016-7037(90)90128-810.1130/b25066.1.

Cui, X., Zhu, W.B., Ge, R.F., 2014. Provenance and crustal evolution of the northern Yangtze block revealed by detrital zircons from neoproterozoic-early paleozoic sedimentary rocks in the Yangtze Gorges area, South China. J. Geol. 122, 217–235. https://doi.org/10.1016/0016-7037(90)90128-810.1086/674801.

Galili, N., Shemesh, A., Yam, R., Brailovsky, I., Sela-Adler, M., Schuster Elaine, M., Collom, C., Bekker, A., Planavsky, N., Macdonald Francis, A., Préat, A., Rudmin, M., Trela, W., Sturesson, U., Heikoop Jeffrey, M., Aurell, M., Ramajo, J., Halevy, I., 2019. The geologic history of seawater oxygen isotopes from marine iron oxides. Science 365 (6452), 469–473. https://doi.org/10.1126/science.aaw9247.

Gilleaudeau, G.J., Sahoo, S.K., Kah, L.C., Henderson, M.A., Kaufman, A.J., 2018. Proterozoic carbonates of the Vindhyan Basin, India: Chemostratigraphy and diagenesis. Gondwana Res. 57, 10–25. https://doi.org/10.1016/j.gr.2018.01.003.

Gu, S., Fu, Y., Long, J., 2019. Predominantly ferruginous conditions in South China during the Marinoan glaciation: Insight from REE geochemistry of the syn-glacial dolostone from the Nantuo Formation in Guizhou Province. China. Minerals 9, 348. https://doi.org/10.1016/0016-7037(90)90128-810.3390/min9060348.

Hoffman, P.F., Abbot, D.S., Ashkenazy, Y., Benn, D.I., Brocks, J.J., Cohen, P.A., Cox, G. M., Creveling, J.R., Donnadieu, Y., Erwin, D.H., Fairchild, I.J., Ferreira, D., Goodman, J.C., Halverson, G.P., Jansen, M.F., Le Hir, G., Love, G.D., Macdonald, F. A., Maloof, A.C., Partin, C.A., Ramstein, G., Rose, B.E.J., Rose, C.V., Sadler, P.M., Tziperman, E., Voigt, A., Warren, S.G., 2017. Snowball Earth climate dynamics and Cryogenian geology-geobiology. Sci. Adv. 3, e1600983 https://doi.org/10.1016/0016-7037(90)90128-810.1126/sciadv.1600983.

Hu, J., Li, C., Tong, J., Ye, Q., Tian, L., An, Z., Dodd, M.S., Algeo, T.J., 2020. Glacial origin of the Cryogenian Nantuo Formation in eastern Shennongjia area (South China): Implications for macroalgal survival. Precambr. Res. 351, 105969 https://doi.org/10.1016/0016-7037(90)90128-810.1016/j.precamres.2020.105969.

Hu, J., Wang, J., Chen, H., Wang, Z., Xie, L., Lin, Q., 2012a. Multiple cycles of glacier advance and retreat during the Nantuo (Marinoan) glacial termination in the Three Gorges area. Frontiers of Earth Science 6, 101–108. https://doi.org/10.1016/0016-7037(90)90128-810.1007/s11707-011-0179-9.

Hu, Z., Liu, Z., Zhang, Y., Mao, X., Ran, R., Liao, Z., Liu, C., 2012b. Determination of the bottom boundary of Shennongjia Group in pre-Nanhuan Period about the northern margin of Yangtze Massif and its geological significance. Resour Environ Eng 3, 201–208. https://doi.org/10.1016/0016-7037(90)90128-810.16536/j.cnki.issn.1671-1211.2012.03.022.

Jacobsen, S.B., Kaufman, A.J., 1999. The Sr, C and O isotopic evolution of Neoproterozoic seawater. Chem. Geol. 161, 37–57. https://doi.org/10.1016/S0009-2541(99)00080-7.

Jiang, G., Shi, X., Zhang, S., Wang, Y., Xiao, S., 2011. Stratigraphy and paleogeography of the Ediacaran Doushantuo Formation (ca. 635–551Ma) in South China. Gondwana Res. 19, 831–849. https://doi.org/10.1016/0016-7037(90)90128-810.1016/j.gr.2011.01.006.

Jiang, G., Sohl, L.E., Christie-Blick, N., 2003. Neoproterozoic stratigraphic comparison of the Lesser Himalaya (India) and Yangtze block (south China): Paleogeographic implications. Geology 31, 917–920. https://doi.org/10.1130/G19790.1.

Kaufman, A., Corsetti, F., Varni, M., 2007. The effect of rising atmospheric oxygen on carbon and sulfur isotope anomalies in the Neoproterozoic Johnnie Formation, Death Valley. USA. Chem. Geol. 237, 47–63. https://doi.org/10.1016/0016-7037(90)90128-810.1016/j.chemgeo.2006.06.023.

Kuang, H., Fan, Z., Liu, Y., Peng, N., Zhu, Z., Yang, Z., Wang, Z., Yu, H.-L., Zhong, Q., 2019. Stromatolite characteristics of Mesoproterozoic Shennongjia Group in the northern margin of Yangtze Block, China. China Geology 2, 362–379. https://doi.org/10.1016/0016-7037(90)90128-810.31035/cg2018115.

Kuang, H., Liu, Y., Peng, N., Vandyk, T.M., Le Heron, D.P., Zhu, Z., Bai, H., Wang, Y., Wang, Z., Zhong, Q., Chen, J., Yu, H., Chen, X., Song, C., Qi, K., 2022. Ediacaran cap dolomite of Shennongjia, northern Yangtze Craton. South China. Precambrian Res. 368, 106483 https://doi.org/10.1016/j.precamres.2021.106483.

Kumar, B., Das Sharma, S., Sreenivas, B., Dayal, A., Rao, M.N., Dubey, N., Chawla, B.R., 2002. Reply—"Carbon, oxygen and strontium isotope geochemistry of Proterozoic

carbonate rocks of the Vindhyan Basin, central India". Precambr. Res. 121, 43–63. https://doi.org/10.1016/S0301-9268(01)00199-1.

Lang, X., Chen, J., Cui, H., Man, L., Huang, K., Fu, Y., Zhou, C., Shen, B., 2018. Cyclic cold climate during the Nantuo Glaciation: Evidence from the Cryogenian Nantuo Formation in the Yangtze Block. South China. Precambrian Res. 310, 243–255. https://doi.org/10.1016/0016-7037(90)90128-810.1016/j.precamres.2018.03.004.

Li, M., 2020. Evaluation of paired carbon isotopic signals from the Ediacaran Doushantuo phosphorites: Diagenetic or primary? Precambr. Res. 349, 105502 https://doi.org/10.1016/0016-7037(90)90128-810.1016/j.precamres.2019.105502.

Liu, P., Yin, C., Chen, S., Tang, F., Gao, L., 2014. The biostratigraphic succession of acanthomorphic acritarchs of the Ediacaran Doushantuo Formation in the Yangtze Gorges area, South China and its biostratigraphic correlation with Australia. Precambr. Res. 225, 29–43. https://doi.org/10.1016/j.precamres.2011.07.009.

Long, J., 2016. Carbonate rocks geochemistry and paleoenvironmental significance of Nantuo ice age in eastern Guizhou. Guizhou University, p. 53.

Lu, S., Ma, G., Gao, Z., Lin, W., 1985. Sinian ice ages and glacial sedimentary facies-areas in China. Precambr. Res. 29, 53–63. https://doi.org/10.1016/0301-9268(85)90059-2.

Lu, S., Qu, L., 1985. The features of glaciogenic rocks of the lower Sinian at Shennongjia region, Hubei Province, with discussion of palaeogeography during the ice ages of early Sinian in Hubei. Bulletin Tianjin Institute of Geology and Mineral Resources 12, 79–102.

Luo, B., 2015. Provenance analysis of glaciogenic class in the Neoproterozoic Nantuo Formation in the eastern Yangtze Gorges area. China University of Geosciences, p. 28.

Qi, L., Xu, Y., Cawood, P., Du, Y., 2018. Reconstructing Cryogenian to Ediacaran successions and paleogeography of the South China Block. Precambr. Res. 314, 452–467. https://doi.org/10.1016/j.precamres.2018.07.003.

Robert, F., Chaussidon, M., 2006. A palaeotemperature curve for the Precambrian oceans based on silicon isotopes in cherts. Nature 443 (7114), 969–972. https://doi.org/10.1038/nature05239.

Sha, Q., Liu, H., Zhang, S., Chen, M., 1963. Nantuo Formation glacial diamictite in the eastern Yangtze Gorges area. Scientia Geologica Sinica 4, 139–148.

Shen, H., Gu, S., Zhao, S., Wu, Z., Feng, Y., 2020. The sedimentary geochemical records of ocean environment during the Nantuo (Marinoan) glaciation in South China—Carbon and oxygen isotopes and trace element compositions of dolostone in Nantuo Formation, Nanhuan System, in eastern Guizhou. Geol. Rev. 66, 214. 10.16509/j.georeview.2020.01.016.

Shen, W., Zhu, X., Yan, B., Qin, H., Gao, Z., Li, F., 2021. Sequence stratigraphy of the Cryogenian Nantuo Formation in South China: Constraints on Marinoan glaciation dynamics. J. Asian Earth Sci. 214, 104776 https://doi.org/10.1016/j.jseaes.2021.104776.

Szpak, P., Metcalfe, J.Z., Macdonald, R.A., 2017. Best practices for calibrating and reporting stable isotope measurements in archaeology. J. Archaeolog. Sci.: Rep. 13, 609–616. https://doi.org/10.1016/j.jasrep.2017.05.007.

Tian, H., Li, H., Liu, H., Zhang, J., Zhou, H., Zhang, K., Xiang, Z., Qu, L., Wang, Z., 2018. Characteristics of C and O isotopes of the Shennongjia group in the margin of the Yangtze Craton and their constraints on paleoenvironment and depositional age. Acta Geol. Sin. 92, 2508–2533.

Trower, E.J., Grotzinger, J.P., 2010. Sedimentology, diagenesis, and stratigraphic occurrence of giant ooids in the Ediacaran Rainstorm Member, Johnnie Formation, Death Valley region. California. Precambrian Res. 180, 113–124. https://doi.org/10.1016/j.precamres.2010.03.007.

Veizer, J., Ala, D., Azmy, K., Bruckschen, P., Buhl, D., Bruhn, F., Carden, G.A.F., Diener, A., Ebneth, S., Godderis, Y., Jasper, T., Korte, C., Pawellek, F., Podlaha, O.G., Strauss, H., 1999. $^{87}Sr/^{86}Sr$, $\delta^{13}C$ and $\delta^{18}O$ evolution of Phanerozoic seawater. Chem. Geol. 161, 59–88. https://doi.org/10.1016/S0009-2541(99)00081-9.

Wang, W., Cawood, P.A., Pandit, M.K., Xia, X., Raveggi, M., Zhao, J., Zheng, J., Qi, L., 2021. Fragmentation of South China from greater India during the Rodinia-Gondwana transition. Geology 49, 228–232. https://doi.org/10.1130/g48308.1.

Xiao, S., Zhou, C., Zhu, M., 2014. International symposium and field workshop on Ediacaran and Cryogenian stratigraphy. Episodes 37 (3), 218–221.

Yang, X., Long, X., Li, J., Dong, Y., Zhao, B., 2020. Mo isotopic response to the end of Neoproterozoic Marinoan glaciation: Evidence from a sedimentary profile in South China. Precambr. Res. 339, 105609 https://doi.org/10.1016/j.precamres.2020.105609.

Ye, Q., Tong, J., Tian, L., Hu, J., An, Z., Bodnar, R.J., Xiao, S., 2019. Detrital graphite particles in the Cryogenian Nantuo Formation of South China: Implications for sedimentary provenance and tectonic history. Precambr. Res. 323, 6–15. https://doi.org/10.1016/j.precamres.2019.01.003.

Ye, Q., Tong, J., Xiao, S., Zhu, S., An, Z., Tian, L., Hu, J., 2015. The survival of benthic macroscopic phototrophs on a Neoproterozoic snowball Earth. Geology 43, 507–510. https://doi.org/10.1130/g36640.1.

Zhang, Q.R., Chu, X., Feng, L.J., 2011. Neoproterozoic glacial records in the Yangtze Region, China, The Geological Record of Neoproterozoic Glaciations. Geological Society of London. Memoirs 357–366. https://doi.org/10.1144/M36.32.

Zhang, S., Jiang, G., Han, Y., 2008. The age of the Nantuo Formation and Nantuo glaciation in South China. Terra Nova 20, 289–294. https://doi.org/10.1111/j.1365-3121.2008.00819.x.

Zhao, J., Zhou, M., Zheng, J., 2013a. Neoproterozoic high-K granites produced by melting of newly formed mafic crust in the Huangling region. South China. Precambrian Res. 233, 93–107. https://doi.org/10.1016/j.precamres.2013.04.011.

Zhao, J., Zhou, M., Zheng, J., Griffin, W.L., 2013b. Neoproterozoic tonalite and trondhjemite in the Huangling complex, South China: Crustal growth and reworking in a continental arc environment. Am. J. Sci. 313, 540. https://doi.org/10.2475/06.2013.02.

Zhao, X., An, Z., Qiu, X., Wu, N., Wei, Y., Hu, K., Zhao, Y., 2018. A new understanding of the "Macaoyuan Group" in north Kongling area of Yangtze Craton. Earth Sci. 43, 3324–3336. https://doi.org/10.3799/dqkx.2018.565.

Zhou, C., Huyskens, M.H., Lang, X., Xiao, S., Yin, Q.-Z., 2019. Calibrating the terminations of Cryogenian global glaciations. Geology 47, 251–254. https://doi.org/10.1130/g45719.1.

Zou, Y., Liu, D., Zhao, F., Kuang, H., Sun, Y., Cheng, J., 2019. Chemostratigraphy of the Mesoproterozoic Shennongjia Group, Yangtze Craton (South China): Implications for oxidized shallow seawaters. J. Asian Earth Sci. 179, 399–415. https://doi.org/10.1016/j.jseaes.2019.02.026.